CAUCHY – Jurnal Matematika Murni dan Aplikasi
Volume 11 (2) (2026), Pages 1910–1931
p-ISSN: 2086-0382; e-ISSN: 2477-3344

Spatiotemporal Dynamics in Predator–Prey Models Incorporating Time Delay and Harvesting

Dede Alif Permana, Diny Zulkarnaen*, and Dian Nuraiman

Department of Mathematics, Faculty of Science and Technology, Universitas Islam Negeri Sunan Gunung Djati Bandung, Indonesia

Abstract

A three–compartment predator–prey model (prey, middle predator, top predator) is developed by integrating spatial diffusion, discrete time delays (biomass conversion and gestation), and proportional harvesting on the two lower trophic levels. The objectives are to formulate the model, analyze local stability dynamics and Hopf bifurcation due to time delay variations, and determine a sustainable harvesting strategy based on the Maximum Sustainable Yield (MSY) concept. Methods include equilibrium analysis, linearization using a variation matrix, Routh–Hurwitz criterion, and numerical simulations with GNU Octave in one–dimensional spatial domains. The results show that a positive interior coexistence equilibrium exists and is locally asymptotically stable under certain conditions. Single or double time delays without harvesting trigger Hopf bifurcation when exceeding critical values, while pure diffusion does not produce instability on its own. Harvesting at safe rates increases the critical delay values and maintains coexistence, in contrast to the mathematical MSY harvesting that leads to species extinction. In conclusion, the integration of diffusion, time delays, and harvesting yields complex dynamics, with time delays as the main destabilizer and controlled harvesting as a stabilizing agent that delays the onset of Hopf bifurcation.

Keywords: Diffusion; Harvesting; Maximum Sustainable Yield (MSY); Three–Compartment Predator–Prey Model; Time Delay.

1. Introduction

The interaction between prey and predator forms a fundamental cornerstone of ecosystem dynamics, with broad practical implications in fisheries, conservation, and pest control [1–9]. While classical Lotka–Volterra models [10, 11] pioneered mathematical ecology, their assumptions of unlimited prey growth and neglect of resource constraints, complex predation, and environmental heterogeneity motivated subsequent developments such as logistic growth, nonlinear functional responses, and multi–trophic structures [1, 3, 5]. Among these, the three-compartment model of Mishra et al. [2] stands out by combining Monod-Haldane and Holling type II responses with diffusion and top-predator cannibalism. In the real world, a three–compartment model can be observed in fishery systems or food chains, such as from plankton to small fish (anchovies/sardines) as prey, tuna and mackerel as middle predators, and sharks as top predators.

However, existing models still overlook two critical biological and anthropogenic realities: (i) inherent time lags in biomass conversion and gestation [4], and (ii) resource harvesting which

*Corresponding author. E-mail: dzulkarnaen@uinsgd.ac.id

Received: June 3, 2026 Revised: July 17, 2026 Accepted: August 14, 2026
DOI: https://doi.org/10.18860/cauchy.v11i2.44741

can fundamentally reshape population dynamics [1, 12, 13]. Time delays are known to trigger oscillatory instabilities (Hopf bifurcation) and chaos, and their interaction with diffusion generates complex spatio-temporal patterns such as travelling waves and stripes that do not arise from either factor alone [7, 14, 15]. Meanwhile, harvesting can either accelerate extinction or, when carefully controlled, serve as a stabilising mechanism [16].

Despite extensive separate studies on diffusion, delays, and harvesting in two-species systems, no work has simultaneously integrated all three into the three–trophic Monod–Haldane/Holling type II framework. This gap motivates our study, which addresses three main questions: (i) formulation of a model incorporating spatial diffusion, two discrete delays, and proportional harvesting; (ii) investigation of equilibrium existence, stability, Hopf bifurcation, and spatio-temporal patterns; and (iii) determination of a harvesting strategy that achieves Maximum Sustainable Yield (MSY) without jeopardising coexistence, while examining how harvesting modifies instability thresholds.

We address these questions via mathematical analysis (linearisation, Routh–Hurwitz criteria, Descartes' rule, transcendental characteristic equations) and numerical simulations using GNU Octave. The main contributions include a unified model integrating diffusion, double delays, and harvesting; a comprehensive local stability and bifurcation analysis with explicit delay thresholds; ecologically safe MSY recommendations that preserve biodiversity; and an exploration of delay-driven spatio-temporal patterns. This study thereby advances mathematical ecology and provides actionable guidance for sustainable resource management. To clarify the original contributions of this research, Table 1 presents a systematic comparison between our model and related studies in the literature.

Table 1: Comparison to earlier studies in literature.

Studies	**Three-Trophic**	**Diffusion**	**Double Delays**	**Harvesting**
Liu et al. [1]	No	Yes	No	Yes
Mishra et al. [2]	Yes	Yes	No	No
Hossain et al. [3]	No	Yes	No	Yes
Yan & Zhang [12]	No	Yes	Yes	Yes
Pal [13]	No	No	Yes	Yes
Majee et al. [14]	No	Yes	Yes	No
Present study	**Yes**	**Yes**	**Yes**	**Yes**

2. Methods

This section describes the mathematical formulation, analytical techniques, and numerical procedures used in this study. The methodology is divided into five parts: model formulation, equilibrium and stability analysis (without delay), maximum sustainable yield (MSY) analysis, stability analysis with time delays, and numerical simulation methods.

2.1. Model Formulation

We consider a three-compartment predator–prey system consisting of prey $x(u,t)$, middle predator $y(u,t)$, and top predator $z(u,t)$, with u as the position vector in two-dimensional space. The basic model, adopted from Mishra et al. [2], includes logistic growth for prey, Monod–Haldane functional response for prey defense, Holling type II response for middle predation, and cannibalism in the top predator. To incorporate spatial movement, we add diffusion terms with Neumann boundary conditions (no-flux) on a bounded domain $\Omega \subset \mathbb{R}^3$. The model is then extended by introducing:

- Proportional harvesting as a constant on prey (h_1) and middle predator (h_2);
- Two discrete time delays: τ_1 for biomass conversion by the middle predator, represents the time required for the middle predator to digest the prey and convert its biomass into new offspring, and τ_2 corresponds to the gestation or maturation period of the top predator.

The resulting system of partial differential equations is:

$$\begin{cases} \dfrac{\partial x}{\partial t} = rx\left(1 - \dfrac{x}{K}\right) - \dfrac{wxy}{bx^2 + a_1} - h_1 x + d_1 \nabla^2 x, \\ \dfrac{\partial y}{\partial t} = \dfrac{w_1 x(t-\tau_1) y}{bx(t-\tau_1)^2 + a_1} - \delta_1 y - \dfrac{\xi yz}{y + a_2} - h_2 y + d_2 \nabla^2 y, \\ \dfrac{\partial z}{\partial t} = \dfrac{\xi_1 y(t-\tau_2) z}{y(t-\tau_2) + a_2} - \delta_2 z - \dfrac{cz^2}{z + a_3} + d_3 \nabla^2 z, \end{cases} \tag{1}$$

with initial conditions $x(\mathbf{u}, 0) > 0,\ y(\mathbf{u}, 0) > 0,\ z(\mathbf{u}, 0) > 0$, for $\mathbf{u} \in \Omega$ and Neumann boundary conditions $\partial x/\partial n = \partial y/\partial n = \partial z/\partial n = 0$ on $\partial\Omega$. All parameters are positive and defined in Table 2.

Table 2: Parameter values used in numerical simulations.

Par.	Description	Value	Source	Unit
r	Intrinsic growth rate of prey.	3.0	Assumed	$1/month$
K	Carrying capacity of prey.	15.0	Assumed	Ton
δ_1	Natural mortality of middle predator.	0.2	[2]	$1/month$
δ_2	Natural mortality of top predator.	0.1	Assumed	$1/month$
a_1	Saturation constant of prey.	15.0	Assumed	Ton
a_2	Saturation constant of middle predator.	15.0	Assumed	Ton
a_3	Half–saturation constant of top predator.	2.0	Assumed	Ton
b	Coefficient of prey defense.	0.05	Assumed	-
w	Reduction rate of prey due to predation.	8.0	Assumed	$1/month$
w_1	Growth rate of middle predator due to predation.	2.0	Assumed	$1/month$
ξ	Reduction rate of middle predator due to predation.	9.0	Assumed	$1/month$
ξ_1	Growth rate of top predator due to predation.	0.8	Assumed	$1/month$
c	Cannibalism rate of top predator.	0.2	[2]	$1/month$

2.2. Equilibrium and Stability Analysis

The positivity and boundedness about this model (1) has been studied in [2]. The addition of the proportional harvesting rate does not alter the invariance of the positive region and two discrete time delays does not affect the positivity and boundedness arguments, but it does affect the stability analysis. We consider the non-diffusive version of system (1) with $d_i = 0$ and without time delays ($\tau_1 = \tau_2 = 0$). The interior equilibrium $E^* = (x^*, y^*, z^*)$, representing the coexistence of all three species, is obtained by solving the following algebraic system when $F_i = 0$ for $i = 1, 2, 3$:

$$\begin{cases} F_1(x, y, z) = r\left(1 - \dfrac{x}{K}\right) - \dfrac{wy}{bx^2 + a_1} - h_1, \\ F_2(x, y, z) = \dfrac{w_1 x}{bx^2 + a_1} - \delta_1 - \dfrac{\xi z}{y + a_2} - h_2, \\ F_3(x, y, z) = \dfrac{\xi_1 y}{y + a_2} - \delta_2 - \dfrac{cz}{z + a_3}. \end{cases} \tag{2}$$

Since we are interested in the interior equilibrium where all populations are positive ($x^*, y^*, z^* > 0$), we can divide each equation by the respective variable. From $F_1 = 0$, we obtain y^* explicitly in terms of x^*:

$$y^* = \frac{(r - h_1)K - rx^*}{Kw}\left(bx^{*2} + a_1\right). \tag{3}$$

From $F_3 = 0$, we obtain z^* explicitly in terms of y^*:

$$z^* = \frac{a_3 y^*(\xi_1 - \delta_2) - a_2 a_3 \delta_2}{y^*(\delta_2 + c - \xi_1) + a_2(\delta_2 + c)}. \tag{4}$$

Substituting (3) and (4) into $F_2 = 0$ and simplifying yields an eighth-degree polynomial in x^*:

$$p_8 x^{*8} + p_7 x^{*7} + p_6 x^{*6} + p_5 x^{*5} + p_4 x^{*4} + p_3 x^{*3} + p_2 x^{*2} + p_1 x^* + p_0 = 0, \tag{5}$$

where the coefficients p_i $(i = 0, 1, \ldots, 8)$ are functions of all model parameters and the harvesting efforts h_1, h_2. The full expressions for p_i are lengthy and are provided in Subsection A.1 for reference. The existence of a positive root of (5) is guaranteed by Descartes' rule of signs. For the parameter set considered in this study (see Table 2), the coefficients exhibit at least one sign change, which ensuring the existence of at least one positive root x^*. Once x^* is determined numerically, there is only one positive real root, then the corresponding y^* and z^* are computed directly from (3) and (4).

To investigate the local stability of the interior equilibrium E^*, we employ the standard linearisation technique. The system (1) without diffusion and delays can be written in the Kolmogorov form:

$$\frac{dx}{dt} = xF_1(x, y, z), \qquad \frac{dy}{dt} = yF_2(x, y, z), \qquad \frac{dz}{dt} = zF_3(x, y, z), \tag{6}$$

where F_1, F_2, and F_3 is from (2).

For such a Kolmogorov-type system, the linearisation around the interior equilibrium E^* is most naturally expressed using the variation matrix V, rather than the standard Jacobian. The variation matrix is given by [2, 17]:

$$V(x^*, y^*, z^*) = \begin{pmatrix} x^*\dfrac{\partial F_1}{\partial x} + F_1 & x^*\dfrac{\partial F_1}{\partial y} & x^*\dfrac{\partial F_1}{\partial z} \\ y^*\dfrac{\partial F_2}{\partial x} & y^*\dfrac{\partial F_2}{\partial y} + F_2 & y^*\dfrac{\partial F_2}{\partial z} \\ z^*\dfrac{\partial F_3}{\partial x} & z^*\dfrac{\partial F_3}{\partial y} & z^*\dfrac{\partial F_3}{\partial z} + F_3 \end{pmatrix}. \tag{7}$$

At the interior equilibrium, the condition $F_1 = F_2 = F_3 = 0$ holds. Consequently, the diagonal entries of the variation matrix simplify, and the matrix takes the form:

$$V = \begin{pmatrix} a_{11} & a_{12} & a_{13} \\ a_{21} & a_{22} & a_{23} \\ a_{31} & a_{32} & a_{33} \end{pmatrix}, \tag{8}$$

where the entries are:

$$\begin{aligned} a_{11} &= -\frac{rx^*}{K} + \frac{2bwx^{*2}y^*}{(bx^{*2} + a_1)^2}, \quad a_{12} = -\frac{wx^*}{bx^{*2} + a_1}, \quad a_{13} = 0 \\ a_{21} &= \frac{w_1 y^*(a_1 - bx^{*2})}{(bx^{*2} + a_1)^2}, \quad a_{22} = \frac{\xi z^* y^*}{(y^* + a_2)^2}, \quad a_{23} = -\frac{\xi y^*}{y^* + a_2}, \\ a_{31} &= 0, \quad a_{32} = \frac{\xi_1 z^* a_2}{(y^* + a_2)^2}, \quad a_{33} = -\frac{cz^* a_3}{(z^* + a_3)^2}. \end{aligned} \tag{9}$$

The characteristic equation of (8) is obtained by solving $\det(\lambda I - V) = 0$.

$$det \begin{vmatrix} \lambda - a_{11} & -a_{12} & 0 \\ -a_{21} & \lambda - a_{22} & -a_{23} \\ 0 & -a_{32} & \lambda - a_{33} \end{vmatrix} = 0.$$

Thus, the characteristic polynomial can be written in the standard cubic form:

$$\lambda^3 + A_1\lambda^2 + A_2\lambda + A_3 = 0, \tag{10}$$

where:

$$\begin{aligned} A_1 &= -(a_{11} + a_{22} + a_{33}), \\ A_2 &= a_{11}a_{22} - a_{12}a_{21} + a_{22}a_{33} - a_{23}a_{32} + a_{11}a_{33}, \\ A_3 &= a_{11}a_{23}a_{32} + a_{12}a_{21}a_{33} - a_{11}a_{22}a_{33}. \end{aligned} \tag{11}$$

By the Routh–Hurwitz criterion, the interior equilibrium E^* is locally asymptotically stable if and only if:

$$A_1 > 0, \qquad A_2 > 0, \qquad A_3 > 0, \qquad A_1A_2 > A_3, \tag{12}$$

additionally, the Routh–Hurwitz conditions are satisfied if the following inequalities hold:

$$(1)\ \frac{2bwx^{*2}y^*}{(bx^{*2}+a_1)^2} < \frac{rx^*}{K}, \quad (2)\ x^{*2} < \frac{a_1}{b}, \quad (3)\ \frac{2bwx^{*2}y^*}{(bx^{*2}+a_1)^2} + \frac{\xi z^* y^*}{(y^*+a_2)^2} < \frac{rx^*}{K} + \frac{cz^* a_3}{(z^*+a_3)^2}$$

These conditions ensure that all eigenvalues have negative real parts, implying that any sufficiently small perturbation from E^* will decay exponentially in time.

For the diffusive system, we consider the full reaction-diffusion system (1) without delays ($\tau_1 = \tau_2 = 0$). To study the stability of the homogeneous steady state E^* against spatial perturbations, we linearise the system and introduce a plane wave perturbation of the form:

$$\begin{pmatrix} x(\eta,t) \\ y(\eta,t) \\ z(\eta,t) \end{pmatrix} = \begin{pmatrix} x^* \\ y^* \\ z^* \end{pmatrix} + \begin{pmatrix} \hat{x} \\ \hat{y} \\ \hat{z} \end{pmatrix} e^{\lambda t + i\mathbf{k}\cdot\eta}, \tag{13}$$

where λ is the temporal growth rate, $\mathbf{k}$ is the wave vector with wavenumber $k = |\mathbf{k}| = \frac{n\pi}{L}$ for $n = 0, 1, 2, ...$, and η is the spatial coordinate. Substituting (13) into the linearised reaction-diffusion system yields the dispersion relation:

$$\det\left(V - k^2 D - \lambda I\right) = 0, \tag{14}$$

where $D = \mathrm{diag}(d_1, d_2, d_3)$ is the diffusion matrix.

The characteristic polynomial for the diffusive system can be written as:

$$\lambda^3 + \Psi_1(k^2)\lambda^2 + \Psi_2(k^2)\lambda + \Psi_3(k^2) = 0, \tag{15}$$

where the coefficients $\Psi_i(k^2)$ are given by:

$$\begin{aligned} \Psi_1(k^2) &= (d_1 + d_2 + d_3)k^2 + A_1, \\ \Psi_2(k^2) &= (d_1d_2 + d_1d_3 + d_2d_3)k^4 \\ &\quad - \left[a_{33}(d_1 + d_2) + a_{22}(d_1 + d_3) + a_{11}(d_2 + d_3)\right]k^2 + A_2, \\ \Psi_3(k^2) &= d_1d_2d_3k^6 - (a_{33}d_1d_2 + a_{22}d_1d_3 + a_{11}d_2d_3)k^4 \\ &\quad + \left[a_{22}a_{33}d_1 - a_{23}a_{32}d_1 + a_{11}a_{33}d_2 + a_{11}a_{22}d_3 - a_{12}a_{21}d_3\right]k^2 + A_3. \end{aligned} \tag{16}$$

The diffusive system is stable against spatial perturbations if, for all $k > 0$, the Routh-Hurwitz conditions for (15) are satisfied:

$$\Psi_1(k^2) > 0, \qquad \Psi_2(k^2) > 0, \qquad \Psi_3(k^2) > 0, \qquad \Psi_1(k^2)\Psi_2(k^2) > \Psi_3(k^2). \tag{17}$$

If these conditions hold for all $k > 0$, then the homogeneous steady state is stable. We also examine whether diffusion alone can destabilize the system by checking conditions (17) for all $k > 0$.

2.3. Maximum Sustainable Yield (MSY) Analysis

The total sustainable yield is defined as the sum of harvested biomass from both harvested species:

$$Y(h_1, h_2) = h_1 x^*(h_1, h_2) + h_2 y^*(h_1, h_2), \tag{18}$$

where (x^*, y^*, z^*) is the interior equilibrium which depends implicitly on the harvesting efforts h_1 and h_2. The concept of Maximum Sustainable Yield (MSY) is central to fisheries and resource management. MSY is defined as the maximum value of $Y(h_1, h_2)$ subject to the constraint that the equilibrium remains positive and locally stable.

To find the MSY, we solve the first-order optimality conditions:

$$\frac{\partial Y}{\partial h_1} = 0, \qquad \frac{\partial Y}{\partial h_2} = 0. \tag{19}$$

Expanding these derivatives using the chain rule yields:

$$\begin{aligned} \frac{\partial Y}{\partial h_1} &= x^* + h_1 \frac{\partial x^*}{\partial h_1} + h_2 \frac{\partial y^*}{\partial h_1} = 0, \\ \frac{\partial Y}{\partial h_2} &= h_1 \frac{\partial x^*}{\partial h_2} + y^* + h_2 \frac{\partial y^*}{\partial h_2} = 0. \end{aligned} \tag{20}$$

Since x^*, y^*, z^* are implicit functions of h_1, h_2, we use implicit differentiation of the equilibrium equations $F_i(x^*, y^*, z^*, h_1, h_2) = 0$ to obtain the required derivatives. Differentiating the system $\mathbf{F} = (F_1, F_2, F_3)^T = 0$ with respect to h_i gives:

$$V \frac{\partial \mathbf{u}^*}{\partial h_i} + \frac{\partial \mathbf{F}}{\partial h_i} = 0, \tag{21}$$

where $\mathbf{u}^* = (x^*, y^*, z^*)^T$ and V is the variation matrix given in (8). Thus, the derivatives of the equilibrium with respect to harvesting efforts are obtained by solving the linear system:

$$\frac{\partial \mathbf{u}^*}{\partial h_i} = -V^{-1} \frac{\partial \mathbf{F}}{\partial h_i}, \qquad i = 1, 2. \tag{22}$$

To confirm that the critical point $(\hat{h}_1, \hat{h}_2)$ obtained from (20) is indeed a local maximum (and not a minimum or saddle point), we examine the second-order conditions. The Hessian matrix of Y is defined as:

$$H(Y) = \begin{pmatrix} \dfrac{\partial^2 Y}{\partial h_1^2} & \dfrac{\partial^2 Y}{\partial h_1 \partial h_2} \\ \dfrac{\partial^2 Y}{\partial h_2 \partial h_1} & \dfrac{\partial^2 Y}{\partial h_2^2} \end{pmatrix}, \tag{23}$$

whose entries are given by:

$$\begin{aligned} \frac{\partial^2 Y}{\partial h_1^2} &= 2\frac{\partial x^*}{\partial h_1} + h_1 \frac{\partial^2 x^*}{\partial h_1^2} + h_2 \frac{\partial^2 y^*}{\partial h_1^2}, \\ \frac{\partial^2 Y}{\partial h_2^2} &= 2\frac{\partial y^*}{\partial h_2} + h_1 \frac{\partial^2 x^*}{\partial h_2^2} + h_2 \frac{\partial^2 y^*}{\partial h_2^2}, \\ \frac{\partial^2 Y}{\partial h_1 \partial h_2} &= \frac{\partial x^*}{\partial h_2} + \frac{\partial y^*}{\partial h_1} + h_1 \frac{\partial^2 x^*}{\partial h_1 \partial h_2} + h_2 \frac{\partial^2 y^*}{\partial h_1 \partial h_2}. \end{aligned} \tag{24}$$

The second-order derivatives $\partial^2 x^*/\partial h_i \partial h_j$ and $\partial^2 y^*/\partial h_i \partial h_j$ can be obtained by differentiating (22) further, or by using finite-difference approximations numerically.

The critical point $(\hat{h}_1, \hat{h}_2)$ is a local maximum if and only if the Hessian matrix is negative definite, i.e.:

$$\frac{\partial^2 Y}{\partial h_1^2} < 0, \qquad \det(H) = \frac{\partial^2 Y}{\partial h_1^2}\frac{\partial^2 Y}{\partial h_2^2} - \left(\frac{\partial^2 Y}{\partial h_1 \partial h_2}\right)^2 > 0. \tag{25}$$

Equivalently, both eigenvalues of $H(Y)$ must be negative.

2.4. Stability Analysis with Time Delays

In this subsection, we investigate the effect of discrete time delays on the stability of the interior equilibrium E^*. We consider the full reaction-diffusion system with delays given in (1). The analysis is divided into two main parts: first, we derive the characteristic equation for the delayed reaction-diffusion system; second, we determine the conditions under which Hopf bifurcation occurs.

2.4.1. Linearisation and Characteristic Equation

To study the local stability of E^*, we introduce small spatio-temporal perturbations around the equilibrium:

$$x(\mathbf{u}, t) = x^* + \hat{x}(\mathbf{u}, t), \qquad y(\mathbf{u}, t) = y^* + \hat{y}(\mathbf{u}, t), \qquad z(\mathbf{u}, t) = z^* + \hat{z}(\mathbf{u}, t), \tag{26}$$

where $|\hat{x}|, |\hat{y}|, |\hat{z}| \ll 1$. Substituting (26) into (1) and retaining only linear terms yields the following linear delay reaction-diffusion system:

$$\frac{\partial}{\partial t}\begin{pmatrix}\hat{x}\\ \hat{y}\\ \hat{z}\end{pmatrix} = A\begin{pmatrix}\hat{x}\\ \hat{y}\\ \hat{z}\end{pmatrix} + B\begin{pmatrix}\hat{x}(t-\tau_1)\\ \hat{y}(t-\tau_1)\\ \hat{z}(t-\tau_1)\end{pmatrix} + C\begin{pmatrix}\hat{x}(t-\tau_2)\\ \hat{y}(t-\tau_2)\\ \hat{z}(t-\tau_2)\end{pmatrix} + D\nabla^2\begin{pmatrix}\hat{x}\\ \hat{y}\\ \hat{z}\end{pmatrix}, \tag{27}$$

where the matrices A, B, C, and D are given by:

$$A = \begin{pmatrix} a_{11} & a_{12} & 0 \\ 0 & a_{22} & a_{23} \\ 0 & 0 & a_{33} \end{pmatrix}, \quad B = \begin{pmatrix} 0 & 0 & 0 \\ b_{21} & 0 & 0 \\ 0 & 0 & 0 \end{pmatrix}, \quad C = \begin{pmatrix} 0 & 0 & 0 \\ 0 & 0 & 0 \\ 0 & c_{32} & 0 \end{pmatrix}, \quad D = \begin{pmatrix} d_1 & 0 & 0 \\ 0 & d_2 & 0 \\ 0 & 0 & d_3 \end{pmatrix}. \tag{28}$$

The coefficients a_{ij} and the delay-related coefficients are:

$$\begin{aligned}
a_{11} &= r\left(1 - \frac{2x^*}{K}\right) - \frac{wy^*(a_1 - bx^{*2})}{(bx^{*2} + a_1)^2}, \quad a_{12} = -\frac{wx^*}{bx^{*2} + a_1}, \\
a_{22} &= -\delta_1 - \frac{\xi z^* a_2}{(y^* + a_2)^2}, \quad a_{23} = -\frac{\xi y^*}{y^* + a_2}, \\
a_{33} &= -\delta_2 - \frac{cz^*(z^* + 2a_3)}{(z^* + a_3)^2}, \\
b_{21} &= \frac{\partial}{\partial x}\left(\frac{w_1 xy}{bx^2 + a_1}\right)\Big|_{E^*} = \frac{w_1 y^*(a_1 - bx^{*2})}{(bx^{*2} + a_1)^2}, \\
c_{32} &= \frac{\partial}{\partial y}\left(\frac{\xi_1 yz}{y + a_2}\right)\Big|_{E^*} = \frac{\xi_1 z^* a_2}{(y^* + a_2)^2}.
\end{aligned} \tag{29}$$

Delay differential equations (DDEs) differ fundamentally from ordinary differential equations in that the rate of change depends on past states. Consequently, solving a DDE requires specifying initial history functions rather than just initial conditions at a single point [18].

Assuming exponential solutions of the form:

$$\begin{pmatrix} \hat{x} \\ \hat{y} \\ \hat{z} \end{pmatrix} = \begin{pmatrix} U \\ V \\ W \end{pmatrix} e^{\lambda t + i\mathbf{k}\cdot\eta}, \tag{30}$$

where $\lambda \in \mathbb{C}$ is the temporal eigenvalue, $\mathbf{k}$ is the wave vector with wavenumber $k = |\mathbf{k}|$, and η is the spatial coordinate. Substituting (30) into (27) yields the characteristic equation:

$$\det\left(\lambda I - A - Be^{-\lambda\tau_1} - Ce^{-\lambda\tau_2} + k^2 D\right) = 0. \tag{31}$$

Expanding the determinant (31) yields the transcendental characteristic equation:

$$P_1(\lambda, k) - P_2(\lambda, k)e^{-\lambda\tau_1} - P_3(\lambda, k)e^{-\lambda\tau_2} + P_4(\lambda, k)e^{-\lambda(\tau_1+\tau_2)} = 0, \tag{32}$$

where the polynomials $P_i(\lambda, k)$ are given by:

$$\begin{aligned} P_1(\lambda, k) &= \lambda^3 - \eta_1(k)\lambda^2 + \eta_2(k)\lambda - \eta_3(k), \\ P_2(\lambda, k) &= \eta_4(k)\lambda^2 - \eta_5(k)\lambda + \eta_6(k), \\ P_3(\lambda, k) &= \eta_7(k)\lambda^2 - \eta_8(k)\lambda + \eta_9(k), \\ P_4(\lambda, k) &= \eta_{10}(k)\lambda - \eta_{11}(k). \end{aligned} \tag{33}$$

where the coefficients η_i $(i = 0, 1, \ldots, 11)$ are provided in Subsection A.1. So we will get another characteristic equation:

$$P_1(\lambda, k) - P_2(\lambda, k)e^{-\lambda\tau_1} - P_3(\lambda, k)e^{-\lambda\tau_2} = 0, \tag{34}$$

Unlike ordinary differential equations, the characteristic equation (34) is transcendental due to the exponential terms $e^{-\lambda\tau_1}$ and $e^{-\lambda\tau_2}$. Consequently, it has infinitely many roots. The local stability of E^* is determined by the location of these roots in the complex plane: the equilibrium is asymptotically stable if and only if all roots have negative real parts ($\mathrm{Re}(\lambda) < 0$).

For the non-diffusive case ($k = 0$), the polynomials in (33) reduce to those given in [2]. However, in this study, we retain the full diffusive form to analyse the combined effects of diffusion and delays on stability.

2.4.2. Hopf Bifurcation Analysis

The presence of time delays can cause roots of the characteristic equation to cross the imaginary axis, leading to a loss of stability and the emergence of periodic solutions through Hopf bifurcation. To detect such bifurcations, we look for purely imaginary roots $\lambda = i\omega$ with $\omega > 0$. Four distinct cases are considered, corresponding to different combinations of the two delays.

Case 1: single delay $\tau_1 > 0$, $\tau_2 = 0$. In this case, the characteristic equation (34) reduces to:

$$\lambda^3 - \alpha_1(k)\lambda^2 + \alpha_2(k)\lambda - \alpha_3(k) - (\beta_1(k)\lambda^2 - \beta_2(k)\lambda + \beta_3(k))e^{-\lambda\tau_1} = 0, \tag{35}$$

where the coefficients are obtained by expanding (33) with $\tau_2 = 0$:

$$\begin{aligned} &\alpha_1(k) = \eta_1(k), \quad \alpha_2(k) = \eta_2(k) + \eta_8(k), \quad \alpha_3(k) = \eta_3(k) + \eta_9(k) \\ &\beta_1(k) = \eta_4(k) = 0, \quad \beta_2(k) = \eta_5(k), \quad \beta_3(k) = \eta_6(k). \end{aligned} \tag{36}$$

Substituting $\lambda = i\omega_1$ $(\omega_1 > 0)$ into (35) and separating real and imaginary parts yields:

$$\begin{aligned} \alpha_1(k)\omega_1^2 - \alpha_3(k) - (\beta_3(k) - \beta_1(k)\omega_1^2)\cos(\omega_1\tau_1) + \beta_2(k)\omega_1\sin(\omega_1\tau_1) = 0, \\ -\omega_1^3 + \alpha_2(k)\omega_1 + (\beta_3(k) - \beta_1(k)\omega_1^2)\sin(\omega_1\tau_1) + \beta_2(k)\omega_1\cos(\omega_1\tau_1) = 0. \end{aligned} \tag{37}$$

Solving (37) for $\sin(\omega_1\tau_1)$ and $\cos(\omega_1\tau_1)$, and using the identity $\sin^2+\cos^2=1$, we obtain a polynomial equation in $\theta=\omega_1^2$:

$$\Theta_1(\theta)=\theta^3+\Psi_1\theta^2+\Psi_2\theta+\Psi_3=0, \tag{38}$$

with:

$$\begin{aligned}\Psi_1&=\alpha_1(k)^2-2\alpha_2(k)-\beta_1(k)^2,\\ \Psi_2&=\alpha_2(k)^2-2\alpha_1(k)\alpha_3(k)-\beta_2(k)^2+2\beta_1(k)\beta_3(k),\\ \Psi_3&=\alpha_3(k)^2-\beta_3(k)^2.\end{aligned} \tag{39}$$

If (38) has at least one positive root θ_0, then $\omega_1^0=\sqrt{\theta_0}$ is a candidate frequency for the Hopf bifurcation. The corresponding critical delay values are then computed as:

$$\tau_1^{(n)}=\begin{cases}\dfrac{1}{\omega_1^0}\left[\cos^{-1}\left(C_1(\omega_1^0)\right)+2n\pi\right], & \text{if } S_1(\omega_1^0)>0,\\[2ex] \dfrac{1}{\omega_1^0}\left[2\pi-\cos^{-1}\left(C_1(\omega_1^0)\right)+2n\pi\right], & \text{if } S_1(\omega_1^0)<0,\end{cases} \qquad n=0,1,2,\ldots \tag{40}$$

where $S_1(\omega_1)$ and $C_1(\omega_1)$ are obtained from (37). The smallest positive value $\tau_1^{(0)}$ is the critical delay at which the first Hopf bifurcation occurs.

To ensure that the Hopf bifurcation is genuine, we must verify the transversality condition:

$$\left.\frac{d(\operatorname{Re}\lambda)}{d\tau_1}\right|_{\tau_1=\tau_1^{(n)}}\neq 0. \tag{41}$$

By implicitly differentiating (35) with respect to τ_1 and evaluating at $\lambda=i\omega_1^0$, one obtains:

$$\operatorname{sign}\left\{\left.\frac{d(\operatorname{Re}\lambda)}{d\tau_1}\right|_{\tau_1=\tau_1^{(n)}}\right\}=\operatorname{sign}\left\{\Theta_1'(\omega_1^0)^2\right\}\neq 0. \tag{42}$$

Thus, the transversality condition is satisfied provided $\Theta_1'(\omega_1^0)^2\neq 0$.

Case 2: single delay $\tau_2>0$, $\tau_1=0$. In this case, the characteristic equation becomes:

$$\lambda^3-\tilde{\alpha}_1(k)\lambda^2+\tilde{\alpha}_2(k)\lambda-\tilde{\alpha}_3(k)-(\tilde{\beta}_1(k)\lambda^2-\tilde{\beta}_2(k)\lambda+\tilde{\beta}_3(k))e^{-\lambda\tau_2}=0, \tag{43}$$

where the coefficients are obtained by expanding (33) with $\tau_1=0$. Following the same procedure as in Case 1, the critical delay τ_2 can be determined as:

$$\tau_2^{(n)}=\begin{cases}\dfrac{1}{\omega_2^0}\left[\cos^{-1}\left(C_2(\omega_2^0)\right)+2n\pi\right], & \text{if } S_2(\omega_2^0)>0,\\[2ex] \dfrac{1}{\omega_2^0}\left[2\pi-\cos^{-1}\left(C_2(\omega_2^0)\right)+2n\pi\right], & \text{if } S_2(\omega_2^0)<0,\end{cases} \qquad n=0,1,2,\ldots \tag{44}$$

where:

$$\sin(\omega_2\tau_2)=\frac{-\tilde{\beta}_2\omega_2(\tilde{\alpha}_1\omega_2^2-\tilde{\alpha}_3)+(\tilde{\beta}_3-\tilde{\beta}_1\omega_2^2)(\omega_2^3-\tilde{\alpha}_2\omega_2)}{\tilde{\beta}_2^2\omega_2^2+(\tilde{\beta}_3-\tilde{\beta}_1\omega_2^2)^2}:=S_2(\omega_2), \tag{45}$$

$$\cos(\omega_2\tau_2)=\frac{-\tilde{\beta}_2\omega_2(\omega_2^3-\tilde{\alpha}_2\omega_2)-(\tilde{\beta}_3-\tilde{\beta}_1\omega_2^2)(\tilde{\alpha}_1\omega_2^2-\tilde{\alpha}_3)}{\tilde{\beta}_2^2\omega_2^2+(\tilde{\beta}_3-\tilde{\beta}_1\omega_2^2)^2}:=C_2(\omega_2), \tag{46}$$

and ω_2^0 be the positive root of the polynomial $\Theta_2(\theta)=\theta^3+\tilde{\Psi}_1\theta^2+\tilde{\Psi}_2\theta+\tilde{\Psi}_3=0$, with $\theta=(\omega_2^0)^2$. For the transversality condition, a similar approach to the previous case is followed as:

$$\operatorname{sign}\left\{\left.\frac{d(\operatorname{Re}\lambda)}{d\tau_2}\right|_{\tau_2=\tau_2^{(n)}}\right\}=\operatorname{sign}\left\{\Theta_2'(\omega_2^0)^2\right\}\neq 0. \tag{47}$$

Thus, the transversality condition is satisfied provided $\Theta_2'(\omega_2^0)^2\neq 0$.

Case 3: combined delays with $\tau_1 > 0$ and τ_2 fixed. In ecological systems, both delays typically operate simultaneously. We now consider the case where τ_2 is fixed at some value (typically below its critical threshold) and τ_1 is varied. Substituting $\lambda = i\omega_3$ into (34) and separating real and imaginary parts yields:

$$l_{11} - m_1 \cos(\omega_3 \tau_1) + n_1 \sin(\omega_3 \tau_1) = 0, \tag{48}$$
$$l_{21} + m_1 \sin(\omega_3 \tau_1) + n_1 \cos(\omega_3 \tau_1) = 0, \tag{49}$$

where the coefficients l_{11}, l_{21}, m_1, n_1 are functions of ω_3, τ_2, and the system parameters (explicit expressions are given in Subsection A.2). Eliminating τ_1 gives a transcendental equation in ω_3:

$$l_{11}^2 + l_{21}^2 - (m_1^2 + n_1^2) = 0. \tag{50}$$

Let ω_3^0 be a positive root of (50). The critical delay τ_1^* is then obtained from:

$$\tau_1^{(n)} = \begin{cases} \dfrac{1}{\omega_3^0}\left[\cos^{-1}\left(C_3(\omega_3^0)\right) + 2n\pi\right], & \text{if } S_3(\omega_3^0) > 0, \\ \dfrac{1}{\omega_3^0}\left[2\pi - \cos^{-1}\left(C_3(\omega_3^0)\right) + 2n\pi\right], & \text{if } S_3(\omega_3^0) < 0, \end{cases} \qquad n = 0, 1, 2, \ldots \tag{51}$$

where S_3 and C_3 are obtained from (48)–(49). The transversality condition is verified by checking:

$$\mathrm{Re}(Q_1)\,\mathrm{Re}(Q_2) + \mathrm{Im}(Q_1)\,\mathrm{Im}(Q_2) \neq 0, \tag{52}$$

where Q_1 and Q_2 are defined in the full derivation (see Subsection A.2).

Case 4: combined delays with τ_1 fixed and $\tau_2 > 0$. This is the symmetric counterpart of Case 3. With τ_1 fixed and τ_2 varied, we substitute $\lambda = i\omega_4$ into (34) and separating real and imaginary parts yields:

$$l_{12} - m_2 \cos(\omega_4 \tau_2) + n_2 \sin(\omega_4 \tau_2) = 0, \tag{53}$$
$$l_{22} + m_2 \sin(\omega_4 \tau_2) + n_2 \cos(\omega_4 \tau_2) = 0, \tag{54}$$

where the coefficients l_{12}, l_{22}, m_2, n_2 are functions of ω_4, τ_1, and the system parameters (are given in Subsection A.2). Eliminating τ_2 gives a transcendental equation in ω_4:

$$l_{12}^2 + l_{22}^2 - (m_2^2 + n_2^2) = 0. \tag{55}$$

Let ω_4^0 be a positive root of (55). The critical delay τ_2^* is then obtained from:

$$\tau_2^{(n)} = \begin{cases} \dfrac{1}{\omega_4^0}\left[\cos^{-1}\left(C_4(\omega_4^0)\right) + 2n\pi\right], & \text{if } S_4(\omega_4^0) > 0, \\ \dfrac{1}{\omega_4^0}\left[2\pi - \cos^{-1}\left(C_4(\omega_4^0)\right) + 2n\pi\right], & \text{if } S_4(\omega_4^0) < 0, \end{cases} \qquad n = 0, 1, 2, \ldots \tag{56}$$

where S_4 and C_4 are obtained from (53)–(54). The transversality condition is verified by checking:

$$\mathrm{Re}(Q_3)\,\mathrm{Re}(Q_4) + \mathrm{Im}(Q_3)\,\mathrm{Im}(Q_4) \neq 0, \tag{57}$$

where Q_3 and Q_4 are defined in the full derivation (see Subsection A.2).

2.4.3. Summary of Hopf Bifurcation Conditions

Based on the analysis above, we summarise the conditions for Hopf bifurcation in the following theorems:

Theorem 1. *For $\tau_2 = 0$, the system (1) undergoes a Hopf bifurcation at the interior equilibrium E^* when $\tau_1 = \tau_1^{(n)}$ $(n = 0, 1, 2, \ldots)$, provided that $\Theta_1'(\omega_1^0)^2 \neq 0$, where Θ_1 is defined in (38) and $\tau_1^{(n)}$ is given by (40).*

Theorem 2. *For $\tau_1 = 0$, the system (1) undergoes a Hopf bifurcation at the interior equilibrium E^* when $\tau_2 = \tau_2^{(n)}$ $(n = 0, 1, 2, \ldots)$, provided that the corresponding transversality condition is satisfied.*

Theorem 3. *For fixed $\tau_2 \in (0, \tau_2^{(0)})$, the system (1) undergoes a Hopf bifurcation at the interior equilibrium E^* when $\tau_1 = \tau_1^{(n)}$ $(n = 0, 1, 2, \ldots)$, provided that (52) holds, where $\tau_1^{(n)}$ is given by (51).*

Theorem 4. *For fixed $\tau_1 \in (0, \tau_1^{(0)})$, the system (1) undergoes a Hopf bifurcation at the interior equilibrium E^* when $\tau_2 = \tau_2^{(n)}$ $(n = 0, 1, 2, \ldots)$, provided that the corresponding transversality condition is satisfied.*

2.4.4. Stability Analysis for the Diffusive Delayed System with Harvesting

When harvesting is included $(h_1, h_2 > 0)$, the analysis proceeds identically with 2.4.1 and 2.4.2. The only modification being that the equilibrium point changes from E^* to $E_h^* = (x_h^*, y_h^*, z_h^*)$, and the coefficients a_{11} and a_{22} in the (29) are replaced by:

$$a_{11}^h = r\left(1 - \frac{2x_h^*}{K}\right) - \frac{wy_h^*(a_1 - bx_h^{*2})}{(bx_h^{*2} + a_1)^2} - h_1, \qquad a_{22}^h = -\delta_1 - \frac{\xi z_h^* a_2}{(y_h^* + a_2)^2} - h_2. \tag{58}$$

All other coefficients are evaluated at the new equilibrium E_h^*. Consequently, the characteristic equation and the Hopf bifurcation conditions have the same structural form, with the modified coefficients. The critical delay values for the harvested system will be denoted by τ_1^{h*} and τ_2^{h*}. As we will demonstrate in Section 3, moderate harvesting increases these critical values, indicating a stabilising effect.

2.5. Numerical Methods

All numerical simulations are performed using GNU Octave version 10.3.0. For spatial domain and discretisation: for 1D simulations, the domain is $[0, L]$ with $L = 100$ (non-delayed) and $L = 20$ (delayed), using 100 grid points ($\Delta x = 1$ for non-delayed or 0.202 for delayed). The non-diffusive ODE system without delay is solved using ode45 (Octave). The PDE system without delay uses a standard Forward Time Centered Space (FTCS) explicit scheme.

The delay ODE system use the method of steps with linear interpolation for the lag values. The maximum step size is limited to $\Delta t_{\max} = \min(0.05, \tau_{\max}/2)$ to ensure accuracy. For the delayed PDE system, we employ an IMEX (Implicit-Explicit) scheme: diffusion is treated implicitly (unconditionally stable), while reaction and delay terms are explicit. The time step is fixed at $\Delta t = 0.05$, which satisfies the stability condition for the explicit part.

History functions for delayed system is defined by small sinusoidal perturbations around the steady state:

$$\begin{aligned} x(u,t) &= x^* + \varepsilon \sin\left(\frac{\pi x}{L}\right)\cos\left(\frac{2\pi x}{L}\right), \\ y(u,t) &= y^* + \varepsilon \cos\left(\frac{2\pi x}{L}\right)\sin\left(\frac{\pi x}{L}\right), \quad t \in [-\tau_{\max}, 0], \\ z(u,t) &= z^* + \varepsilon \sin\left(\frac{3\pi x}{L}\right)\cos\left(\frac{\pi x}{L}\right), \end{aligned} \tag{59}$$

with $\varepsilon = 0.1$. For the system with delay, the value of $x(t-\tau)$ is calculated as: (1) perform linear interpolation using interp1 (Octave) on the stored historical data, (2) taken directly from the time index $n - round(\tau/dt)$, that is, the zero-order hold approximation. This is a common approach for computational efficiency.

All simulations use initial conditions consisting of small perturbations around the equilibrium point: (1) without delay, $x(0) = 1.5, y(0) = 0.8, z(0) = 0.5$ for ODE system and $x(u,0) = x^* + 0.1\cos(\frac{2\pi x}{L})$ for PDE system, (2) delayed system, using a sinusoidal perturbations $x(u,t) = x^*(1 + 0.1\sin(\frac{\pi x}{L})\cos(\frac{2\pi x}{L}))$.

3. Results and Discussion

This section presents the main findings from the analytical and numerical investigations. We organise the results into six subsections covering stability of the basic model, MSY, effects of time delays, spatio-temporal patterns, the stabilising role of harvesting, and a general discussion.

3.1. Stability of the Basic Model

For the parameters in Table 2, the non-diffusive system without harvesting or delay admits a unique stable interior equilibrium $E^* = (5.5018,\ 3.9212,\ 0.9804)$, reflecting top-down regulation and cannibalistic control. The characteristic polynomial $\lambda^3 + 0.6997\lambda^2 + 1.0513\lambda + 0.0885 = 0$ satisfies the Routh–Hurwitz ($A_1 > 0, A_2 > 0, A_3 > 0, A_1A_2 > A_3$), confirming local asymptotic stability. The 3D phase portrait and population dynamics over time (Fig. 1) show convergence to this equilibrium.

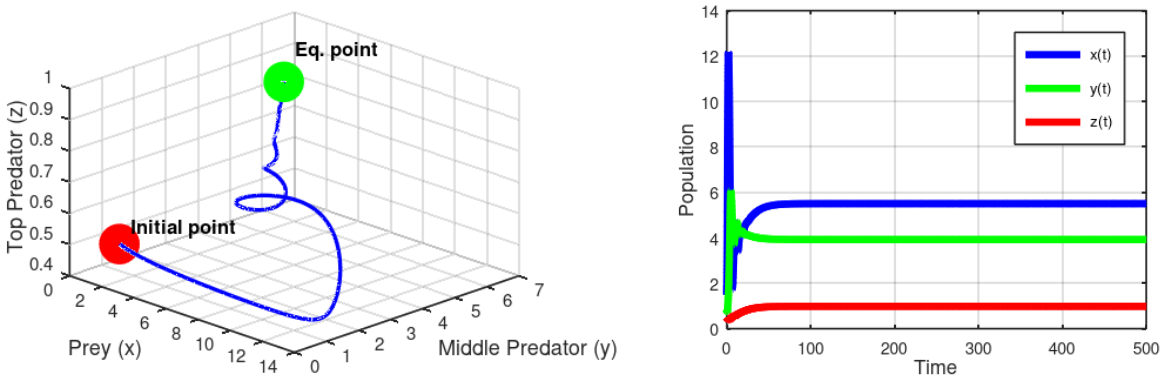

(a) **(b)**

Fig. 1: (a) 3D phase portrait. (b) Time evolution over population densities.

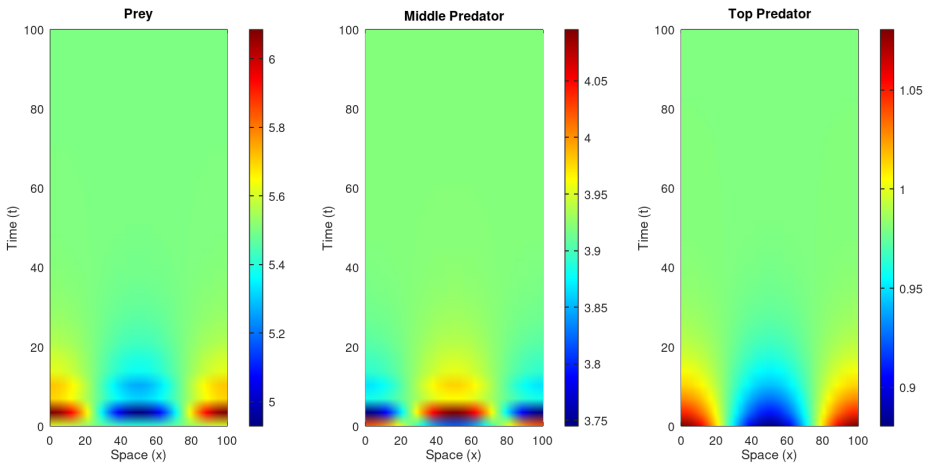

Fig. 2: Spatio-temporal distribution showing homogeneous state.

In the diffusive system, the parameter values used are, of course, the same and refer to Table 2. However, since this is a model that incorporates diffusion, there are additional parameter values for the diffusion coefficients. The values $d_1 = 1$, $d_2 = 0.025$, and $d_3 = 3$ were selected, taken from [2]. Thus diffusion acts solely as damping, producing no instability. This is validated numerically in Fig. 2, where initial perturbations decay monotonically to a uniform state, confirming that without delays the system is robust to spatial heterogeneity.

3.2. Maximum Sustainable Yield (MSY)

The yield function $Y(h_1, h_2)$ was maximised numerically. The unconstrained maximum occurs at $(\hat{h}_1, \hat{h}_2) = (1.469,\ 2.204)$ with $Y_{\max} = 11.2453$ (Fig. 3a). The Hessian at this point is negative definite, so it is a local maximum. However, the coexistence equilibrium is $(7.6531,\ 10^{-20},\ 10^{-22})$– the middle and top predators on the brink of extinction. This mathematical MSY is theoretically true, but ecologically unsustainable because it destroys biodiversity. This result highlights a critical limitation of the classical MSY concept when applied to multi-trophic systems, which can inadvertently promote ecosystem collapse rather than sustainable exploitation.

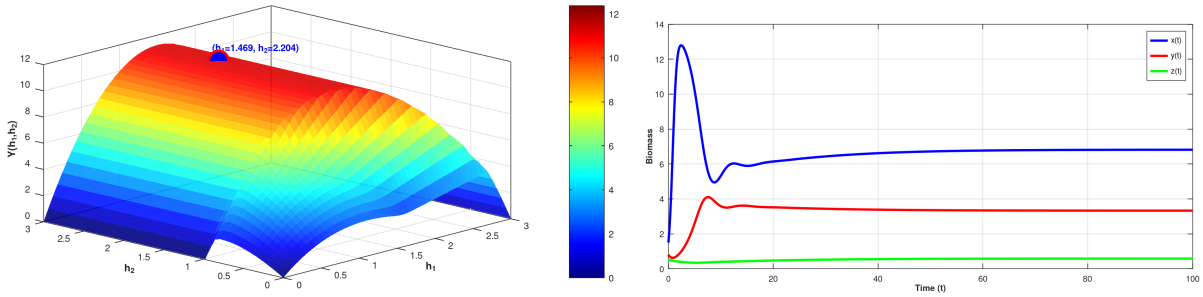

(a) **(b)**

Fig. 3: (a) Yield function $Y(h_1, h_2)$ showing the MSY point. (b) Time evolution over biomass under the safe harvesting strategy $(0.1, 0.3)$.

To maintain coexistence, we choose a safer harvesting strategy $(h_1^*, h_2^*) = (0.1,\ 0.3)$, which gives a higher positive equilibrium $(6.8177,\ 3.3272,\ 0.5846)$, indicating that all three trophic levels persist—albeit with a slightly elevated prey density and reduced predator densities compared to the unharvested state (Fig. 3b). The corresponding sustainable yield is $Y = 1.6799$, which is approximately six times smaller than the theoretical MSY. Although this yield is much lower than the mathematical maximum, it preserves all three species and maintains local stability. Moreover, as we will rigorously demonstrate in Section 3.5, this moderate harvesting actually increases the system's resilience to time delays.

3.3. Effects of Time Delays (Without Diffusion)

We first consider the non-diffusive delayed system without harvesting.

Single delay τ_1 (with $\tau_2 = 0$): The characteristic equation yields a critical value $\tau_1^* = 0.6191$. For $\tau_1 < 0.6191$ (e.g., $\tau_1 = 0.5$), trajectories dampen to E^* (Fig. 4a). For $\tau_1 > 0.6191$ (e.g., $\tau_1 = 1.0$), the system loses stability and exhibits persistent periodic oscillations (Hopf bifurcation) (Fig. 4b). The amplitude increases with τ_1. This behaviour confirms Theorem 1, which guarantees the occurrence of Hopf bifurcation when τ_1 crosses τ_1^*.

Single delay τ_2 (with $\tau_1 = 0$): The critical value is much larger: $\tau_2^* = 148.8016$. For $\tau_2 < \tau_2^*$ (e.g., 100), the system remains stable (Fig. 5a); for $\tau_2 > \tau_2^*$ (e.g., 200), periodic oscillations appear (Fig. 5b). This large difference indicates that the system is far more sensitive to the biomass-conversion delay (τ_1) than to the top-predator gestation delay (τ_2). This is in full agreement with Theorem 2, where the critical threshold τ_2^* marks the onset of periodic oscillations.

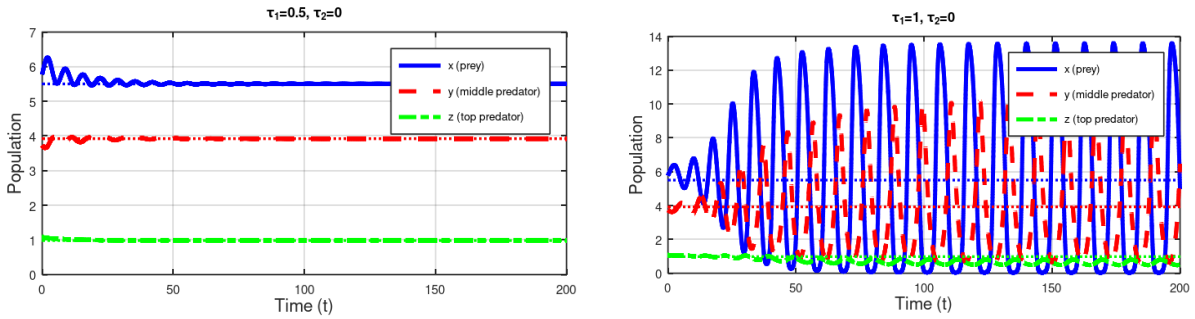

(a) **(b)**

Fig. 4: Dynamics with varying $\tau_1 > 0$ and $\tau_2 = 0$. (a) $\tau_1 = 0.5$, $\tau_2 = 0$. (b) $\tau_1 = 1$, $\tau_2 = 0$.

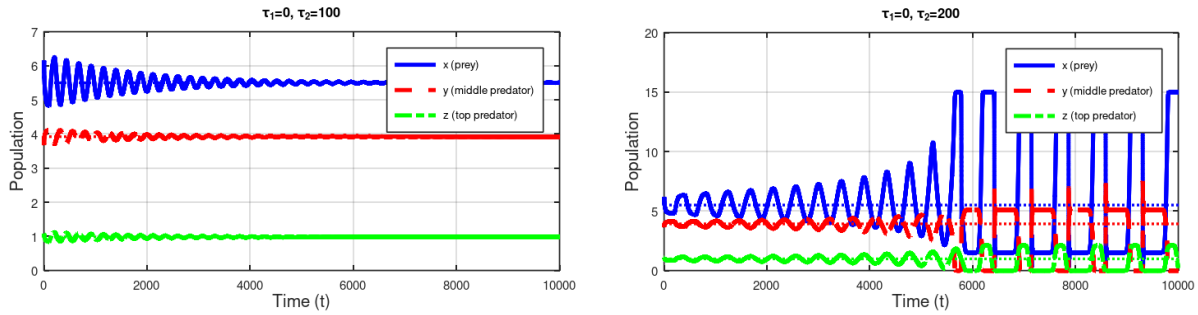

(a) **(b)**

Fig. 5: Dynamics with varying $\tau_1 = 0$ and $\tau_2 > 0$. (a) $\tau_1 = 0$, $\tau_2 = 100$. (b) $\tau_1 = 0$, $\tau_2 = 200$.

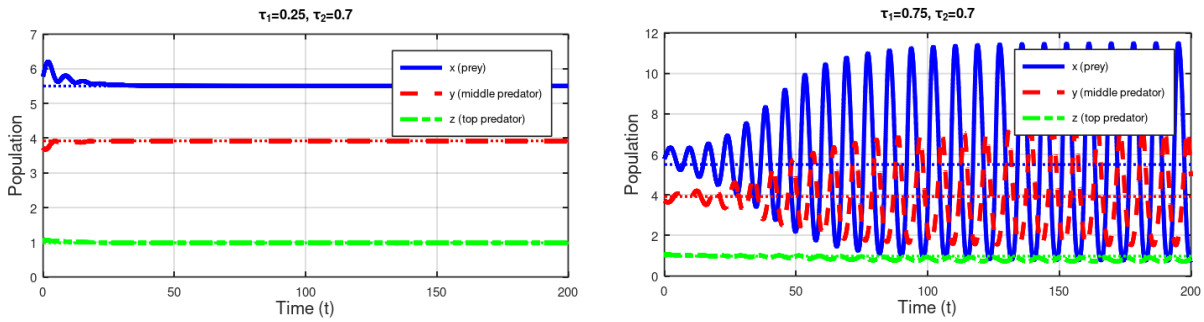

(a) **(b)**

Fig. 6: Dynamics with varying $\tau_1 > 0$ and τ_2 fixed. (a) $\tau_1 = 0.25$, $\tau_2 = 0.7$. (b) $\tau_1 = 0.75$, $\tau_2 = 0.7$.

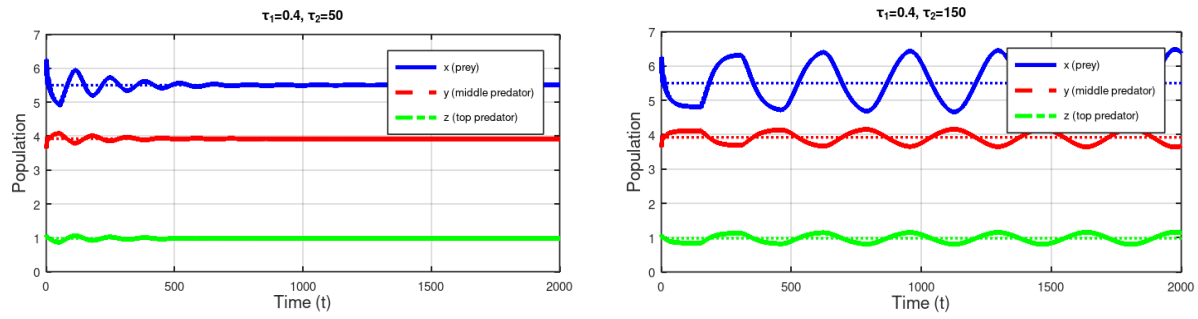

(a) **(b)**

Fig. 7: Dynamics with varying τ_1 fixed and $\tau_2 > 0$. (a) $\tau_1 = 0.4$, $\tau_2 = 50$. (b) $\tau_1 = 0.4$, $\tau_2 = 150$.

Double delays: When both delays are active, the critical thresholds decrease. For $\tau_2 = 0.7$ fixed, the critical threshold decreases from $\tau_1^* = 0.6191$ to 0.5812 (Fig. 6). This result validates Theorem 3, which states that the presence of a fixed τ_2 reduces the critical value of τ_1. Similarly, with $\tau_1 = 0.4$ fixed, τ_2^* decreases from 148.8016 to 146.9179 (Fig. 7). This observation is consistent with Theorem 4, confirming that a fixed τ_1 lowers the threshold for τ_2-induced instability.

3.4. Spatio-temporal Patterns with Diffusion and Delays

When diffusion is added, the system with delays below the critical values ($\tau_1^* = 0.6191$ and $\tau_2^* = 148.8016$) still converges to a homogeneous steady state (no patterns) Fig. 8. However, when a delay exceeds its critical value, the Hopf oscillations interact with spatial diffusion to produce delay-driven instability and form complex spatio-temporal patterns.

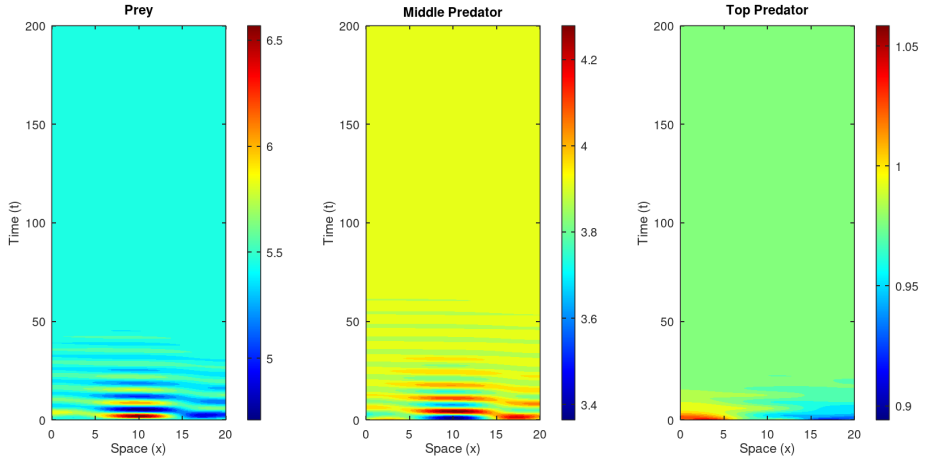

Fig. 8: Contour plot for $\tau_1 = 0.5$, $\tau_2 = 0$: homogeneous.

For $\tau_1 > \tau_1^*$ (with $\tau_2 = 0$), we observe travelling waves and stripe-like patterns (Fig. 9). This spatio-temporal instability arises from the interplay between diffusion and the Hopf bifurcation established in Theorem 1. For $\tau_2 > \tau_2^*$ (with $\tau_1 = 0$), similar patterns emerge, but with longer wavelengths (Fig. 10). These patterns are a direct consequence of the Hopf bifurcation predicted by Theorem 2, now modulated by spatial dispersal.

For double delays, the patterns appear sooner and exhibit more intricate structures (Fig. 11). For $\tau_2 = 0.7$ fixed, the critical value is $\tau_1^* = 0.5812$. For $\tau_1 = 0.4$ fixed, $\tau_2^* = 146.9179$. The combined delays produce multi-scale patterns with both short and long wavelengths, reflecting the superposition of oscillations from both trophic levels. The earlier onset of patterns under double delays corroborates Theorem 3 and Theorem 4, where the interaction of both delays accelerates the loss of spatial homogeneity.

3.5. Role of Harvesting as a Stabilising Factor

Remarkably, introducing moderate harvesting $(h_1, h_2) = (0.1, 0.3)$ significantly raises the critical delay thresholds:

1. τ_1^* increases from 0.6191 to 1.0738 (an increase of $\approx 73\%$).
2. τ_2^* increases from 148.8016 to 166.1013 (an increase of $\approx 12\%$).
3. For $\tau_2 = 0.8$ fixed, τ_1^* rises from 0.5812 to 1.0409.
4. For $\tau_1 = 0.6$ fixed, τ_2^* rises from 146.9179 to 159.7422.

Simulations confirm that with harvesting, the system remains stable for delay values that would otherwise trigger oscillations. This demonstrates that the modified critical thresholds, predicted by the harvested versions of Theorem 1 and Theorem 2, effectively delay the Hopf bifurcation. For example, with $\tau_1 = 0.8$ and $\tau_2 = 0$, the unharvested system would be unstable,

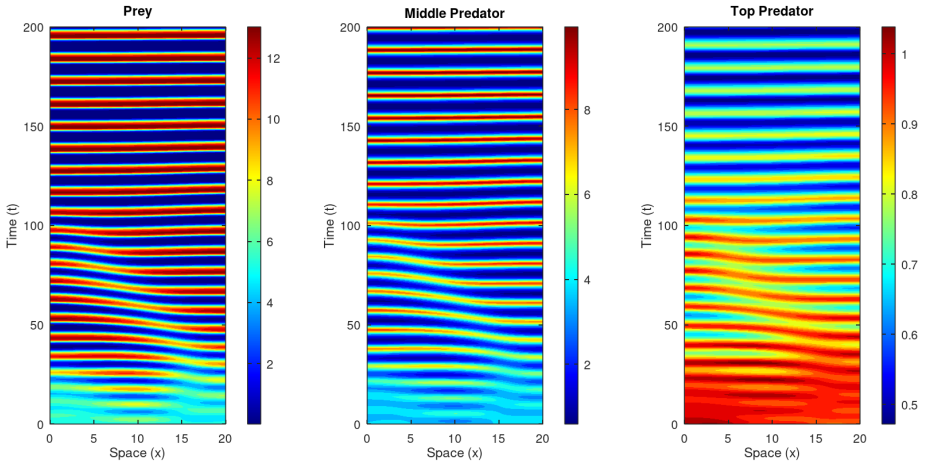

Fig. 9: Contour plot for $\tau_1 = 1.0$, $\tau_2 = 0$: travelling waves.

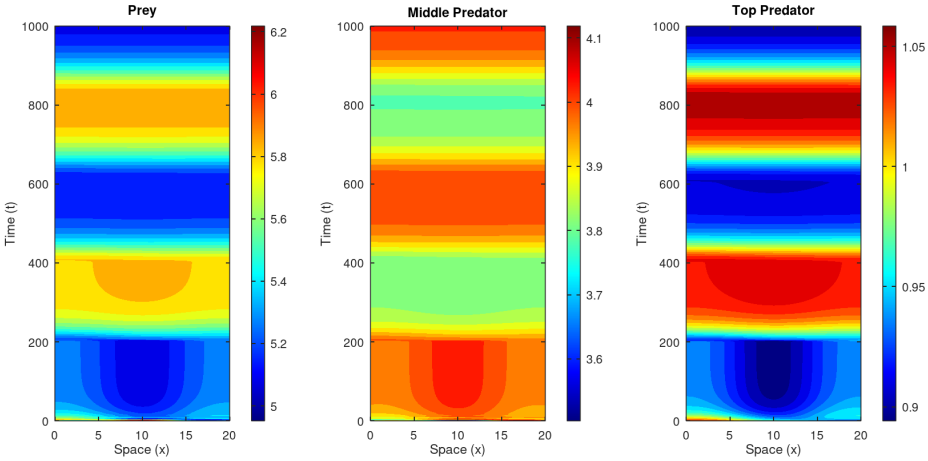

Fig. 10: Contour plot for $\tau_1 = 0$, $\tau_2 = 200$: stripes.

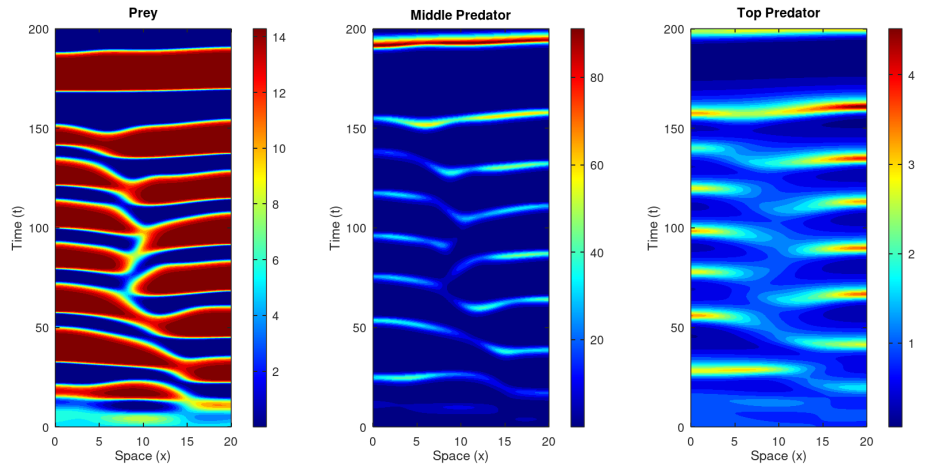

Fig. 11: Contour plot for $\tau_1 = 3$, $\tau_2 = 0.7$: waves and stripes.

but the harvested system is stable (Fig. 12). Only when τ_1 exceeds the new, higher threshold (e.g., $\tau_1 = 2.0$) do we see oscillations and patterns (Fig. 13). For the harvested system with both delays active, the reduced critical thresholds are consistent with Theorem 3 and Theorem 4 adapted to the harvested equilibrium. The resulting contour plots with both delays are qualitatively similar to those shown in Fig. 12 and Fig. 13.

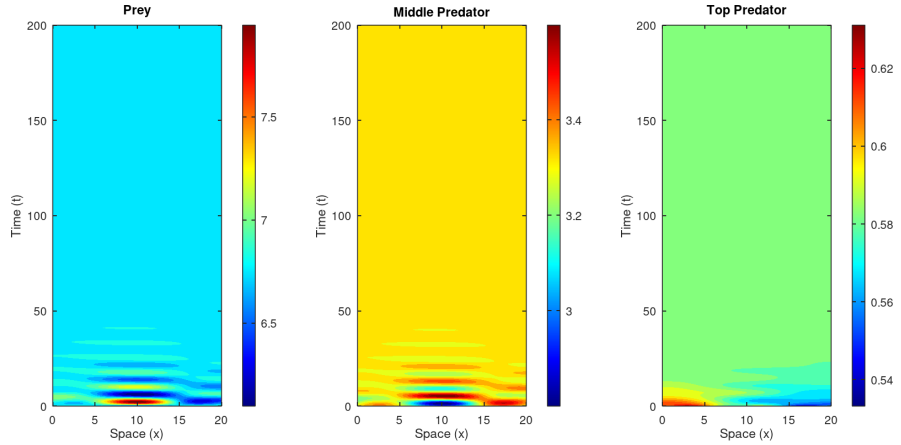

Fig. 12: Contour with harvesting: $\tau_1 = 0.8$, $\tau_2 = 0$: stable.

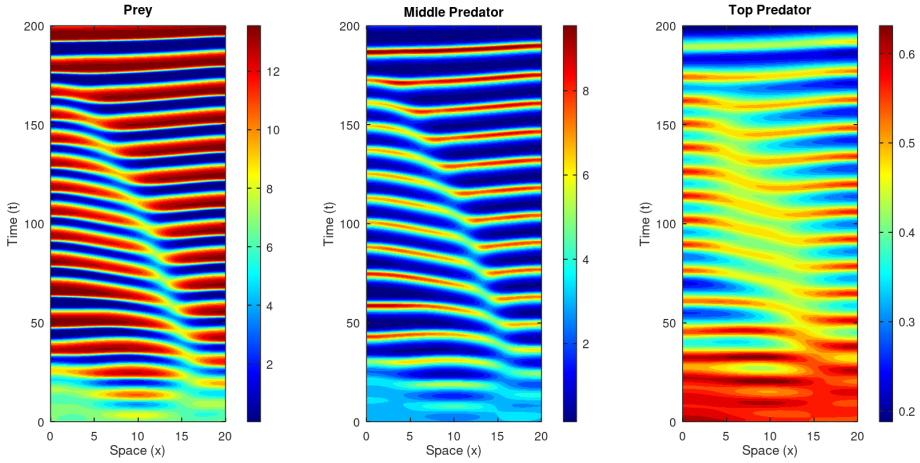

Fig. 13: Contour with harvesting: $\tau_1 = 2.0$, $\tau_2 = 0$: patterns.

Our results demonstrate that the interplay among spatial diffusion, discrete time delays, and proportional harvesting generates rich dynamics in a three-trophic food web. Diffusion alone does not induce spatial instability, corroborating Mishra et al. [2], whereas time delays act as potent destabilising agents. Notably, the biomass-conversion delay (τ_1) exerts a far stronger influence than the top-predator gestation delay (τ_2), aligning with biological expectations as rapid physiological processes have narrower tolerance windows before triggering oscillatory instabilities.

Harvesting analysis reveals a critical trade-off: theoretical MSY maximises total yield but eradicates top predators, whereas a conservative strategy (0.1, 0.3) preserves all three species and provides a sustainable catch. More surprisingly, moderate harvesting acts as a stabilising mechanism by raising critical delay values, thereby attenuating positive feedback loops that would otherwise amplify delayed oscillations. When super-critical delays combine with diffusion, the system self-organises into complex spatio-temporal structures such as travelling waves and stripes, characteristic of delay-driven instability in reaction-diffusion systems [7, 15].

Comparisons with related studies [3, 14] highlight that our three-trophic structure provides a more comprehensive picture, where stabilising harvesting contrasts with destabilising effects reported in some two-species models [12]. Despite limitations such as constant discrete delays and theoretical parameters, the qualitative insights remain robust and lay a foundation for future work with field data, alternative functional responses, and economic optimisation (MEY).

4. Conclusion

In this study, we successfully formulated and analysed a three-compartment predator-prey model integrating spatial diffusion, two discrete delays (biomass conversion and gestation), and proportional harvesting. The proposed system, given by (1), extends the classical Mishra et al. [2] framework. For the chosen parameters, we established a unique positive interior equilibrium $E^* = (5.5018,\ 3.9212,\ 0.9804)$ that is locally asymptotically stable, and the diffusive system remains stable against spatial perturbations under these conditions.

Our MSY analysis reveals a fundamental dilemma: the mathematically optimal effort $(h_1, h_2) = (1.469,\ 2.204)$ maximises biomass but drives predators to extinction, whereas an ecologically safe strategy $(0.1,\ 0.3)$ maintains all three species with a sustainable yield $Y = 1.6799$. Time delays are the primary source of instability, with Hopf bifurcations at $\tau_1^* = 0.6191$ and $\tau_2^* = 148.8016$. Crucially, moderate harvesting significantly elevates these thresholds to $\tau_1^* = 1.0738$ and $\tau_2^* = 166.1013$, acting as a buffer against biological time lags.

The interaction of super-critical delays with spatial diffusion leads to complex spatio-temporal patterns, revealing the relationship between temporal instabilities and spatial dispersal. Our research indicates that effectively managed harvesting can stabilize ecosystems, fostering long-term species coexistence. These findings provide essential theoretical insights for sustainable resource management, while also suggesting pathways for economic optimization, varied functional responses, and empirical validation. Additionally, dispersion curves, spectral analysis, and sensitivity analysis could support these assertions across a wider range of harvesting parameters.

CRediT Authorship Contribution Statement

Dede Alif Permana: Conceptualization, Methodology, Software, Validation, Formal Analysis, Writing - Original Draft, Visualization. **Diny Zulkarnaen:** Conceptualization, Methodology, Supervision, Writing - Review & Editing, Project Administration, Funding Acquisition. **Dian Nuraiman:** Supervision, Writing - Review & Editing.

Declaration of Generative AI and AI-assisted technologies

The authors used AI-assisted writing tools during the preparation of this manuscript. Specifically, DeepSeek (by DeepSeek Company) and Gemini (by Google) were used only for language editing and grammatical refinement. No AI-generated content contributed to the conceptual development, theoretical formulation, or substantive research contributions of the paper.

Declaration of Competing Interest

The authors declare no competing interests.

Funding and Acknowledgments

This research was made possible through the research funding provided by Department of Mathematics, Faculty of Science and Technology, Universitas Islam Negeri Sunan Gunung Djati Bandung in 2026. We sincerely thank them for their support.

The authors would also like to express their sincere gratitude to Dr. Arief Fatchul Huda and Elvi Syukrina Erianto, M. Si., for their invaluable feedback, constructive criticism, and thorough review during the examination of the first author's undergraduate thesis, which significantly contributed to refining the analysis and improving the overall quality of this manuscript.

Data and Code Availability

The data and code supporting the findings of this study are available from the corresponding author upon reasonable request and subject to confidentiality agreements.

References

[1] G. Liu, Z. Chang, X. Meng, and S. Liu. "Optimality for a diffusive predator-prey system in a spatially heterogeneous environment incorporating a prey refuge". In: *Applied Mathematics and Computation* 384 (2020). DOI: 10.1016/j.amc.2020.125385.

[2] P. Mishra, S.N. Raw, and B. Tiwari. "On a cannibalistic predator–prey model with prey defense and diffusion". In: *Applied Mathematical Modelling* 90 (2021), pp. 165–190. DOI: 10.1016/j.apm.2020.08.060.

[3] S. Hossain, Md. Manarul Haque, M. H. Kabir, M. O. Gani, and S. Sarwardi. "Complex spatio temporal dynamics of a harvested prey–predator model with Crowley–Martin response function". In: *Results in Control and Optimization* 5 (2021). DOI: 10.1016/j.rico.2021.100059.

[4] H. Jiang, S. Gao, and H. Wang. "Predator-prey dynamics with personality-dependent foraging and maturation delay stability switches, Hopf and Bogdanov-Takens bifurcations". In: *Mathematical Biosciences* 393 (2026). DOI: 10.1016/j.mbs.2025.109609.

[5] S. Vinoth, R. Sivasamy, K. Sathiyanathan, B. Unyong, G. Rajchakit, R.Vadivel, and N. Gunasekaran. "The dynamics of a Leslie type predator–prey model with fear and Allee effect". In: *Advances in Difference Equations* 338 (2021). DOI: 10.1186/s13662-021-03490-x.

[6] A. Acharya, A. Mahata, N. Sil, S. Mahato, S. Mukherjee, Sanat K. Mahato, and B. Roy. "A prey-refuge harvesting model using intuitionistic fuzzy sets". In: *Decision Analytics Journal* 8 (2023). DOI: 10.1016/j.dajour.2023.100308.

[7] Sasanka S. Maity, S. Roy, and Pankaj K. Tiwari. "Spatio-temporal dynamics of a predator–prey system with variable carrying capacity and Cosner response function". In: *Franklin Open* 11 (2025). DOI: 10.1016/j.fraope.2025.100289.

[8] T. Ravichandran, M. M. Tajudeen K. Asmiya Banu, F. S. Alshammari, G. Rajchakit, and A. Akgul. "Optimizing a delayed predator-prey model to account for infection in both populations". In: *Results in Control and Optimization* 23 (2026). DOI: 10.1016/j.rico.2026.100680.

[9] D. Tripathi, J. P. Tripathi, S. K. Tiwari, D. Jana, Li-Feng Hou, Yu Shi, Gui-Quan Sun, V. Tiwari, and J. K. K. Asamoah. "Modified Holling Tanner diffusive and non-diffusive predator–prey models: The impact of prey refuge and fear effect". In: *Results in Physics* 65 (2024). DOI: 10.1016/j.rinp.2024.107995.

[10] Alfred J. Lotka. *Elements of Physical Biology*. William & Wilkins Company, 1925. https://archive.org/details/elementsofphysic017171mbp/page/n5/mode/2up.

[11] Vito Volterra. "Variations and Fluctuations of the Number of Individuals in Animal Species living together". In: *Journal de Counsil* 3.1 (1926), pp. 3–51. https://jxshix.people.wm.edu/2009-harbin-course/classic/Volterra-1928.pdf.

[12] Xiang-Ping Yan and Cun-Hua Zhang. "Global stability of a delayed diffusive predator–prey model with prey harvesting of Michaelis–Menten type". In: *Applied Mathematics Letters* 114 (2021). DOI: 10.1016/j.aml.2020.106904.

[13] A. K. Pal. "Controlling chaotic dynamics of a delayed Hassell–Varley type predator–prey model with non-linear harvesting efforts in prey by using imprecise biological parameters". In: *Results in Control and Optimization* 14 (2024). DOI: 10.1016/j.rico.2023.100361.

[14] S. Majee, S. Jana, T. K. Kar, R. Anand, and J. Ramprabhakar. "Impact of incubation and gestation periods on the dynamics of a spatially heterogeneous eco-epidemiological model". In: *Scientific Reports* 15.19661 (2025). DOI: 10.1038/s41598-025-02778-2.

[15] N. B. Sharmilaa, Gunasundari C., S. M. Boulaaras, and Suvitha V. "Diffusion and distributed delay effects in a predator–prey system:A mathematical analysis". In: *Partial Differential Equations in Applied Mathematics* 10 (2024). DOI: 10.1016/j.padiff.2024.100709.

[16] Paulo Rebelo and Silvério Rosa. "An optimal control problem for a predator–prey model with strong and weak preys". In: *Chaos, Solitons and Fractals* 191 (2025). DOI: 10.1016/j.chaos.2024.115838.

[17] J. D. Murray. *Mathematical Biology I: An Introduction*. Springer, 2002. https://link.springer.com/book/10.1007/b98868.

[18] Andrei D. Polyanin, Vsevolod G. Sorokin, and Alexei I. Zhurov. *Delay Ordinary and Partial Differential Equations*. CRCPress, 2023. https://www.researchgate.net/publication/368575153_Delay_Ordinary_and_Partial_Differential_Equations.

A. Appendix

A.1. Polynomial Coefficients

$$
\begin{aligned}
p_8 &= (\delta_1+h_2)b^3r^2(c+\delta_2-\xi_1)\\
p_7 &= -b^2r(c+\delta_2-\xi_1)\left(2K(r-h_1)(\delta_1+h_2)b+rw_1\right),\\
p_6 &= -b^2\left(-c-\delta_2+\xi_1\left(b(r-h_1)^2(\delta_1+h_2)K^2\ +2rw_1(r-h_1)K+3r^2a_1(\delta_1+h_2)\right)\right),\\
p_5 &= \left(-2br^2(c+\delta_2-\xi_1)w_1+6b^2Kr(h_1-r)(\delta_1+h_2)(c+\delta_2-\xi_1)\right)a_1\\
&\quad -b^2Kr(\delta_1+h_2)(2c+2\delta_2-\xi_1)wa_2+b^2Ka_3r\xi(\delta_2-\xi_1)w\\
&\quad -b^2K^2(h_1-r)^2(c+\delta_2-\xi_1)w_1,\\
p_4 &= 3br^2(\delta_1+h_2)(c+\delta_2-\xi_1)a_1^2\\
&\quad +bK(h_1-r)(c+\delta_2-\xi_1)\left(3Kb(h_1-r)(\delta_1+h_2)-4rw_1\right)a_1\\
&\quad -bKw(2c+2\delta_2-\xi_1)\left(Kb(h_1-r)(\delta_1+h_2)-rw_1\right)a_2+b^2K^2a_3w\xi(h_1-r)(\delta_2-\xi_1),\\
p_3 &= \left(-r^2(c+\delta_2-\xi_1)w_1+6Kbr(h_1-r)(\delta_1+h_2)(c+\delta_2-\xi_1)\right)a_1^2\\
&\quad +(-2Kbrw(\delta_1+h_2)(2c+2\delta_2-\xi_1)a_2+2Ka_3br\xi(\delta_2-\xi_1)w\\
&\quad -2K^2b(h_1-r)^2(c+\delta_2-\xi_1)w_1\Big)a_1+K^2bww_1(h_1-r)(2c+2\delta_2-\xi_1)a_2,\\
p_2 &= r^2(\delta_1+h_2)(c+\delta_2-\xi_1)a_1^3\\
&\quad +\left(3K^2(h_1-r)^2(\delta_1+h_2)(c+\delta_2-\xi_1)b\ -2Krw_1(h_1-r)(c+\delta_2-\xi_1)\right)a_1^2\\
&\quad +\Big(\Big(Krw_1(2c+2\delta_2-\xi_1)-2K^2b(h_1-r)(\delta_1+h_2)(2c+2\delta_2-\xi_1)\Big)wa_2\\
&\quad +2K^2a_3bw\xi(h_1-r)(\delta_2-\xi_1)\Big)a_1+K^2bw^2(\delta_1+h_2)(c+\delta_2)a_2^2-K^2a_3bw^2\xi\delta_2a_2,\\
p_1 &= -2Kr(h_1-r)(\delta_1+h_2)(c+\delta_2-\xi_1)a_1^3+(Krw(\delta_1+h_2)(2c+2\delta_2-\xi_1)a_2\\
&\quad +Ka_3r\xi(\delta_2-\xi_1)w-K^2(h_1-r)^2(c+\delta_2-\xi_1)w_1\Big)a_1^2\\
&\quad +K^2ww_1(h_1-r)(2c+2\delta_2-\xi_1)a_2a_1-K^2w^2w_1(c+\delta_2)a_2^2,\\
p_0 &= K^2(h_1-r)^2(\delta_1+h_2)(c+\delta_2-\xi_1)a_1^3+\Big(-K^2w(h_1-r)(\delta_1+h_2)(2c+2\delta_2-\xi_1)a_2\\
&\quad +K^2a_3w\xi(h_1-r)(\delta_2-\xi_1)\Big)a_1^2+\Big(K^2w^2(\delta_1+h_2)(c+\delta_2)a_2^2-K^2a_3w^2\xi\delta_2a_2\Big)a_1,\\
\eta_1(k) &= a_{11}+a_{22}+a_{33}-(d_1+d_2+d_3)k^2,\\
\eta_2(k) &= a_{11}a_{22}+a_{11}a_{33}+a_{22}a_{33}-\{a_{33}(d_1+d_2)+a_{22}(d_1+d_3)+a_{11}(d_2+d_3)\}k^2\\
&\quad +(d_1d_2+d_1d_3+d_2d_3)k^4,\\
\eta_3(k) &= a_{11}a_{22}a_{33}-(a_{22}a_{33}d_1+a_{11}a_{33}d_2+a_{11}a_{22}d_3)k^2\\
&\quad +(a_{33}d_1d_2+a_{22}d_1d_3+a_{11}d_2d_3)k^4-d_1d_2d_3k^6,\\
\eta_4(k) &= b_{22}=0,\\
\eta_5(k) &= -a_{12}b_{21},\\
\eta_6(k) &= -a_{12}a_{33}b_{21}+a_{12}b_{21}d_3k^2,\\
\eta_7(k) &= c_{33}=0,\\
\eta_8(k) &= a_{11}c_{33}+a_{22}c_{33}-a_{13}c_{31}-a_{23}c_{32}-c_{33}(d_1+d_2)k^2=-a_{23}c_{32},\\
\eta_9(k) &= -a_{11}a_{23}c_{32}+a_{23}c_{32}d_1k^2,\\
\eta_{10}(k) &= b_{22}c_{33}=0,\\
\eta_{11}(k) &= a_{11}b_{22}c_{33}+a_{13}b_{21}c_{32}-a_{12}b_{21}c_{33}-a_{13}b_{22}c_{31}-b_{22}c_{33}d_1k^2=0.
\end{aligned}
$$

A.2. Coefficients of Delay Case 3 and 4

$$
\begin{aligned}
l_{11} &= \eta_1\omega_3^2 - \eta_3 + (\eta_7\omega_3^2 - \eta_9)\cos(\tau_2\omega_3) + \eta_8\omega_3\sin(\tau_2\omega_3),\\
l_{12} &= \eta_1\omega_4^2 - \eta_3 + (\eta_4\omega_4^2 - \eta_6)\cos(\tau_1\omega_4) + \eta_5\omega_4\sin(\tau_1\omega_4),\\
l_{21} &= -\omega_3^3 + \eta_2\omega_3 + \eta_8\omega_3\cos(\tau_2\omega_3) - (\eta_7\omega_3^2 - \eta_9)\sin(\tau_2\omega_3),\\
l_{22} &= -\omega_4^3 + \eta_2\omega_4 + \eta_5\omega_4\cos(\tau_1\omega_4) - (\eta_4\omega_4^2 - \eta_6)\sin(\tau_1\omega_4),\\
m_1 &= -\eta_4\omega_3^2 + \eta_6 - \eta_{10}\omega_3\sin(\tau_2\omega_3) + \eta_{11}\cos(\tau_2\omega_3),\\
m_2 &= -\eta_7\omega_4^2 + \eta_9 - \eta_{10}\omega_4\sin(\tau_1\omega_4) + \eta_{11}\cos(\tau_1\omega_4),\\
n_1 &= \eta_5\omega_3 + \eta_{10}\omega_3\cos(\tau_2\omega_3) + \eta_{11}\sin(\tau_2\omega_3),\\
n_2 &= \eta_8\omega_4 + \eta_{10}\omega_4\cos(\tau_1\omega_4) + \eta_{11}\sin(\tau_1\omega_4),\\
Q_1(\omega_3^0,\tau_1^0) &= \Big\{(P_2P_3 + P_1P_4)\sin(\tau_2\omega_3^0) - P_3P_4\sin(2\tau_2\omega_3^0)\Big\}\\
&\quad - i\left\{P_1P_2 - (P_2P_3 + P_1P_4)\cos(\tau_2\omega_3^0) + P_3P_4\cos(2\tau_2\omega_3^0)\right\},\\
Q_2(\omega_3^0,\tau_1^0) &= P_2\eta_2 + P_1\eta_5 + P_1P_2\tau_1 - 3P_2(\omega_3^0)^2 + \{-P_4\eta_2 - P_3\eta_5 + P_2\eta_8 - P_2P_3\tau_1 + P_2P_3\tau_2\\
&\quad + P_1(-P_4(\tau_1+\tau_2)) + 3P_4(\omega_3^0)^2\}\cos(\tau_2\omega_3^0) - (P_4\eta_8 - P_3P_4\tau_1)\cos(2\tau_2\omega_3^0)\\
&\quad + (2P_4\eta_1 + 2P_3\eta_4 - 2P_2\eta_7)\omega_3^0\sin(\tau_2\omega_3^0) + 2P_4\eta_7\omega_3^0\sin(2\tau_2\omega_3^0)\\
&\quad + i\Big\{-2P_2\eta_1\omega_3^0 - 2P_1\eta_4\omega_3^0 + 2(P_4\eta_1 + P_3\eta_4 - P_2\eta_7)\omega_3^0\cos(\tau_2\omega_3^0)\\
&\quad + 2P_4\eta_7\omega_3^0\cos(2\tau_2\omega_3^0) + (P_4\eta_2 + P_3\eta_5 - P_2\eta_8 + P_2P_3\tau_1\\
&\quad + P_1P_4\tau_1 - P_2P_3\tau_2 + P_1P_4\tau_2 - 3P_4(\omega_3^0)^2)\sin(\tau_2\omega_3^0)\\
&\quad + (P_4\eta_8 - P_3P_4\tau_1)\sin(2\tau_2\omega_3^0)\Big\},\\
Q_3(\omega_4^0,\tau_2^0) &= (P_2P_3 + P_1P_4)\sin(\tau_1\omega_4^0) - P_2P_4\sin(2\tau_1\omega_4^0)\\
&\quad - i\left\{P_1P_3 - (P_2P_3 + P_1P_4)\cos(\tau_1\omega_4^0) + P_2P_4\cos(2\tau_1\omega_4^0)\right\},\\
Q_4(\omega_4^0,\tau_2^0) &= P_3\eta_2 + P_1\eta_8 + P_1P_3\tau_2 - 3P_3(\omega_4^0)^2 + \{-P_4\eta_2 + P_3\eta_5 - P_2\eta_8 + P_2P_3\tau_1 - P_2P_3\tau_2\\
&\quad + P_1(-P_4(\tau_1+\tau_2)) + 3P_4(\omega_4^0)^2\}\cos(\tau_1\omega_4^0) - (P_4\eta_5 - P_2P_4\tau_2)\cos(2\tau_1\omega_4^0)\\
&\quad + (2P_4\eta_1 - 2P_3\eta_4 + 2P_2\eta_7)\omega_4^0\sin(\tau_1\omega_4^0) + 2P_4\eta_4\omega_4^0\sin(2\tau_1\omega_4^0)\\
&\quad + i\Big\{-2P_3\eta_1\omega_4^0 - 2P_1\eta_7\omega_4^0 + 2(P_4\eta_1 - P_3\eta_4 + P_2\eta_7)\omega_4^0\cos(\tau_1\omega_4^0)\\
&\quad + 2P_4\eta_4\omega_4^0\cos(2\tau_1\omega_4^0) + (P_4\eta_2 - P_3\eta_5 + P_2\eta_8 - P_2P_3\tau_1\\
&\quad + P_1P_4\tau_1 + P_2P_3\tau_2 + P_1P_4\tau_2 - 3P_4(\omega_4^0)^2)\sin(\tau_1\omega_4^0)\\
&\quad + (P_4\eta_5 - P_2P_4\tau_2)\sin(2\tau_1\omega_4^0)\Big\}.
\end{aligned}
$$